SAFETY OF BUILDING CRITICAL INFRASTRUCTURES AND TERRITORIES

DOI 10.15826/rjcst.2021.2.001 УДК 69.04

S. A. Timashev[1,2], *N. A. Lavrov*[1]
[1]Science and Engineering Centre «Reliability and Safety of Large Systems and Machines», Ural Branch, Russian Academy of Sciences, Ekaterinburg, Russia
[2]Ural Federal University, Ekaterinburg, Russia
E-mail: timashevs@gmail.com

GEOMETRIC POSITIONING RELIABILITY OF SPACECRAFT CANTILEVER STRUCTURES

Abstract. The paper describes the results of assessing reliability of spacecraft cantilever structures (SCS) that serve as supports of radio reflectors. The specifics of SCS reliability is that they should be capable of serving 12-15 years in space without changing their 3D geometry. Results of reliability calculation of two types of lattice cantilever carbon polymer beams are presented. Further needed research is suggested.

Key words: spacecraft, cantilever structures, reliability, positioning accuracy

С. А. Тимашев[1,2], *Н. А. Лавров*[1]
[1]Научно-инженерный центр «Надежность и безопасность больших систем и машин», Уральское отделение Российской академии наук, Екатеринбург, Россия
[2] Уральский федеральный университет, Екатеринбург, Россия
E-mail: timashevs@gmail.com

НАДЕЖНОСТЬ ГЕОМЕТРИЧЕСКОГО ПОЗИЦИОНИРОВАНИЯ КОНСОЛЬНЫХ КОНСТРУКЦИЙ КОСМИЧЕСКИХ АППАРАТОВ

Аннотация. В статье описываются результаты оценки надежности консольных конструкций космических аппаратов (ККА), служащих опорами радиоотражателей. Специфика надежности ККА заключается в том, что они должны быть способны прослужить 12-15 лет в космосе без изменения своей 3D-геометрии. Представлены результаты расчета надежности двух типов решетчатых консольных углеродных полимерных балок. Предлагаются дальнейшие необходимые исследования.

Ключевые слова: космический аппарат, консольные конструкции, надежность, точность позиционирования.

Introduction

The modern concept of spacecraft design is based on creating objects with a body controlled in flight and flexible cantilever structures attached to it, which are deployed or assembled on a given orbit.

Controlled telecommunication satellites are typical representatives of unique spacecraft with a rigid body, to which flexible cantilever structures (solar panels, radio-technical antennas, and remote instrument rods) are attached, designed to operate in zero gravity [1].

The main purpose of cantilever structures (CS) is to provide a given positioning accuracy of working surfaces with photo-converting or radio-reflecting equipment. These CS must also have a certain stiffness that excludes unwanted deformations in orbit that allows the spacecraft on-board systems to effectively perform their specified functions.

The task of designing the spacecraft cantilever elements is achieving specified accuracy and stiffness parameters values in the operating position and maintaining those permissible values by the end of the spacecraft active life (12-15 years) in orbit.

Achievement of the specified values of CS parameters is carried out during their design, mainly by choosing proper structural materials, structural connections, structural layout, structural power schemes and applying rational design principles [2].

To ensure reliability, it is required to predict structure behavior, taking into account the degradation of its initial parameters during all phases of its life cycle (LC): during its launch to the orbit as a part of a launch vehicle and deployment in orbit; when moving the spacecraft from the reference orbit to the work orbit; during the period of its active operation.

The operational reliability of large-sized structures of modern long-term operation spacecraft according to accuracy and rigidity criteria by the end of their active life should be at least 0.999.

The method for calculating the deployment reliability and failure-free operation of the spacecraft CS was first developed in 1978 [3–4] and has not lost its relevance so far. Since the mid-seventies, considerable experience has been accumulated in ensuring the reliability of opening consoles, which is reflected in foreign standards MIL-A-83577, DOD-A-83577A, MIL-A-83577B, OCT 92-4339–80, NASA-STD-5017, AIAA S-114–2005, NASA-STD-5017A, ECSS-E-30 Part 3A and ECSS-E-ST-33-01C. The methodology for assessing reliability of the deployment of individual spacecraft consoles is given in [5]

Life cycle of a cantilever structure

The standard life cycle of a spacecraft CS consists of the following phases:

- fabrication of the structure at the manufacturing plant;
- carrying out control and acceptance tests of the structure;
- installation and fastening of the rod in folded state onto the spacecraft;
- storage and ground transportation of the spacecraft in folded position;
- installation of the spacecraft on the rigid body of the launch vehicle;
- spacecraft flight as part of a launch vehicle into a near-earth orbit;
- decoupling, turning and fixing of the spacecraft rod in the operating position;
- operating the rod as a console under the influence of following outer space factors: (1) vacuum, (2) weightlessness, (3) daily temperature cycles, (4) high radiation and (5) propulsion systems operation loads when launching into the design orbit, and correcting the orientation and 3D position of the spacecraft.

In accordance with the standard life cycle of the spacecraft CS, the inevitable random structural factors that exist during the creation of the console and affect the structure operation are: (1) the spread of physical and mechanical characteristics of materials and geometric imperfections of the rod (deviations from the design dimensions during manufacture); (2) errors in adjusting and weight-balancing of the rod; (3) climatic conditions; (4) loading the structure in the folded position in the launch area.

The factors that randomly change during the active life of the structure are: (5) cyclic heat loads and other environmental influences; (6) backlash in connections; (7) material properties (due to degradation).

The vector sum of all instability factors of the spacecraft CS should not exceed a given value Δ at any moment of its active existence in orbit (12-15 years).

Structure description

Within this article, a cantilever design of an antenna system with a reflector is considered, which ensures its detachment from the spacecraft.

This problem is solved with the help of a rod, which in the folded state has dimensions that allow it to be placed on the spacecraft under the rocket fairing. In unfolded position, the rod should provide the required distance from the spacecraft to the reflector fixed at its end (Fig. 1).

The rod consists of a transformable frame, which is a strut structure that in deployed position consists of a set of identical sections. Each section has the shape of a parallelepiped with diagonal bars on its sides. The rod contains (1) a drive for deployment of the transformable frame, (2) end and root mechanisms that provide the required angular position of the reflector relative to the spacecraft.

The longitudinal bars of each section can be folded. A spring mechanism with stops is mounted inside the struts that works in conjunction with the strut deployment drive and ensures stability of the struts in the deployed position (Fig. 2).

Diagonal bars provide the required tensional rigidity of the rod in the unfolded position. They have a telescopic design and are fixed in the deployed position with spring-loaded conical latches (Fig. 3).

The transformation of the struts of one cell in the process of unfolding the rod is shown in Fig. 4.

Research problem statement

Consider the influence of thermal deformations of the spacecraft rod in the operating position on the change in its geometric shape, caused by the influence of the near-earth orbit environment.

In order to do this, calculate the linear displacements of the antenna attachment points to the rod at the maximum temperature change for two types of rods – with a square cross-section (the cell is a parallelepiped with a square base and diagonals on the outer sides, Fig. 5) and with a triangular cross-section (the cell is a prism with a triangular base and diagonals on the outer sides, Fig. 6).

Initial data for the research problem

The problem is solved for the following initial data:

- standard temperature cycle for spacecraft in near-earth orbit: from –160°C to +135°C;
- initial temperature of the rod: + 20°C (it is assumed that at this temperature the rod has no deformations);
- the rod length: 20, 50 and 100 *m*, with a mesh length of 1 *m*; the height and width of the square cells is 670 *mm*, the height and length of the triangular base is 670 *mm*;
- rod material - carbon fiber (a composite polymer material);
- the material modulus of elasticity adopted for calculations is 200 GPa;
- the temperature coefficient of its linear expansion is insufficiently studied and is, according to [7-10], in the range $[2\cdot10^{-6}\ °C^{-1} \dots -2\cdot10^{-6}\ °C^{-1}]$ taking into account the relaxation of the material. For calculation, the worst case is accepted as $2\cdot10^{-6}\ °C^{-1}$;
- all struts of the rod are of tubular section, with nominal pipe bore 20 *mm*, and wall thickness 1 *mm*.

Calculation description

The calculation of the displacements of the antenna mount section was performed for two load cases:

- for minimum temperature –160°C (total temperature change relative to "zero" deformation temperature $\Delta T = 20 - (-160) = 180°C$);

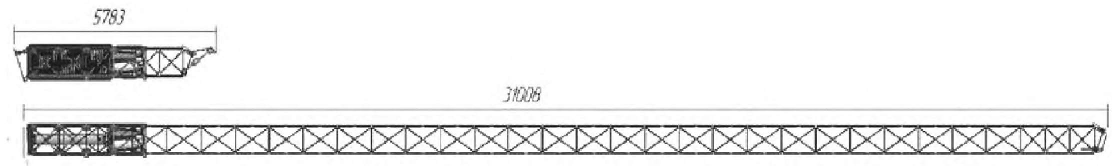

Fig. 1. An example of a rod in folded and unfolded states

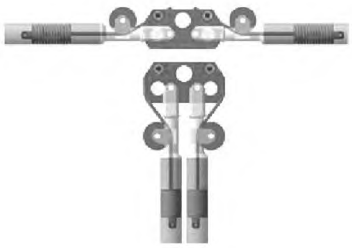

Fig. 2. Variant of the longitudinal bar opening unit [6]

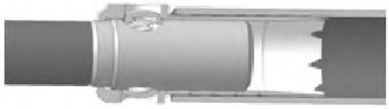

Fig. 3. A variant of the mechanism for fixing the opening of the telescopic rod [6]

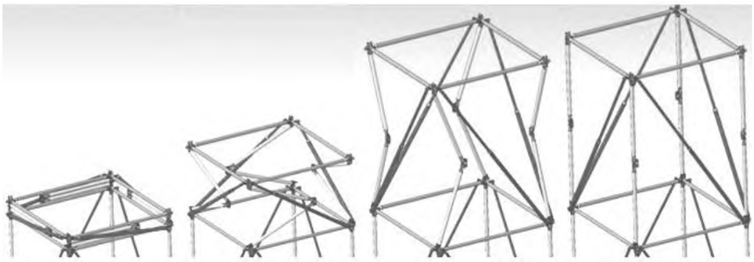

Fig. 4. Variant of the rod cell deployment process [6]

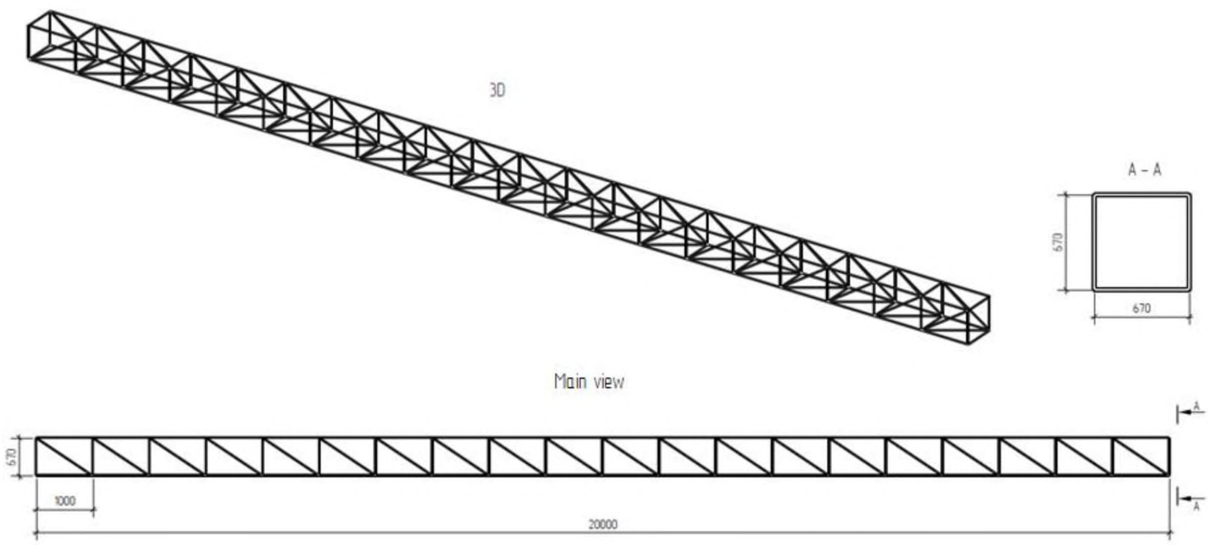

Fig. 5. Rod with square cross-section

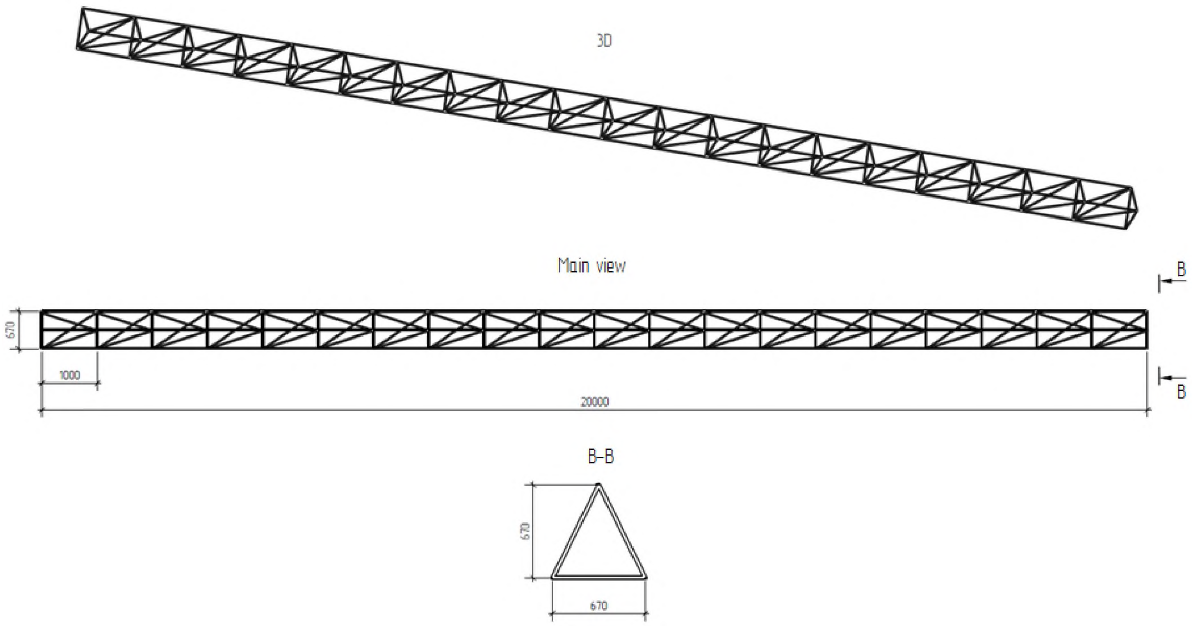

Fig. 6. Rod with triangular cross-section

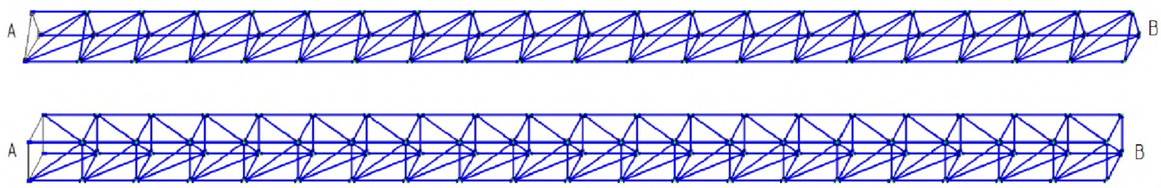

Fig. 7. Design schemes of two types of rods

- for maximum temperature +135°C (total temperature change relative to "zero" deformation temperature $\Delta T = 135 - 20 =$ $= 115$°C

Design schemes

Fig. 7 shows the design schemes for the rods in the ЛИРА-САПР 2016 program. The displacements of the root section A points are equal to zero. The displacements of the points of section B where the antenna is attached to the rod must be found for both cases of thermal expansion. All bars are simply hinged to each other.

A load in the form of thermal expansion is applied to all struts of the rod according to the loadings and characteristics of the rod material discussed above. The stiffness of the struts is determined according to the characteristics of the sections and the material of the struts.

Maximum permissible values of rod deformations

The maximum permissible deviations of the rod geometry are:

- angular rotation relative to the axes of the coordinate system – no more than ± 0.2°;
- linear displacement relative to the longitudinal X-axis, no more than ± 10.0 mm.

Calculation results for uniform temperature deformations

Table 1 shows the results of calculations of temperature deformations for different rod types.

Calculation results and comparison with maximal permissible displacements

According to Table 1 the linear displacement size along the X- axis of the rod due to its uniform temperature deformations does not depend (as expected) on the shape of the structure.

With given length of the rod. the maximal permissible displacement along its X-axis is reached with following temperature changes: length 20 *m*:

$$\Delta T = \frac{\pm 10 \cdot 10^{-3}}{20 \cdot 2 \cdot 10^{-6}} = \pm 250 \text{ K};$$

– length 50 *m*:

$$\Delta T = \frac{\pm 10 \cdot 10^{-3}}{50 \cdot 2 \cdot 10^{-6}} = \pm 100 \text{K};$$

– length 100 *m*:

$$\Delta T = \frac{\pm 10 \times 10^{-3}}{100 \times 2 \times 10^{-6}} = \pm 50 \text{K}.$$

Table 1

Calculation results

Rod type	Points	Displacement, *mm*						Rotation around X-axis, 10^{-4} *radian*	
		X-axis		Y-axis		Z-axis			
		T max	*T min*	*T max*	*T min*	*T max*	*T min*	*T max*	*T min*
Square cross-section. length 20 *m*	B1	4.6	-7.2	-0.1541	0.2412	0.1541	-0.2412	2.3	3.6
	B2	4.6	-7.2	0	0	0	0		
	B3	4.6	-7.2	0.1541	-0.2412	-0.1541	0.2412		
	B4	4.6	-7.2	0	0	0	0		
Square cross-section. length 50 *m*	B1	11.5	-18	-0.1541	0.2412	0.1541	-0.2412	2.3	3.6
	B2	11.5	-18	-1.31 E-08	2.05 E-08	0	1.46 E-08		
	B3	11.5	-18	0.1541	-0.2412	-0.1541	0.2412		
	B4	11.5	-18	1.82 E-08	-2.84 E-08	2.19 E-08	-3.43 E-08		
Square cross-section. length 100 *m*	B1	23	-36	-0.1541	0.2412	0.1541	-0.2412	2.3	3.6
	B2	23	-36	-1.01 E-07	1.58 E-07	-3.04 E-07	4.75 E-07		
	B3	23	-36	0.1541	-0.2412	-0.1541	0.2412		
	B4	23	-36	-1.59 E-07	2.49 E-08	-3.62 E-07	5.67 E-07		
Triangular cross-section. length 20 *m*	B1	4.6	-7.2	0	0	0	0	1.2	1.8
	B2	4.6	-7.2	0	0	0.1926	-0.3015		
	B3	4.6	-7.2	0.1541	-0.2412	0.07705	-0.1206		
Triangular cross-section. length 50 *m*	B1	11.5	-18	0	0	0	0	1.2	1.8
	B2	11.5	-18	0	0	0.19263	-0.3015		
	B3	11.5	-18	0.1541	-0.2412	0.07705	-0.1206		
Triangular cross-section. length 100 *m*	B1	23	-36	2.07 E-07	-3.26 E-07	-3.46 E-07	5.41 E-07	1.2	1.8
	B2	23	-36	2.04 E-07	-3.22 E-07	0.19263	-0.3015		
	B3	23	-36	0.1541	-0.2412	0.07705	-0.1206		

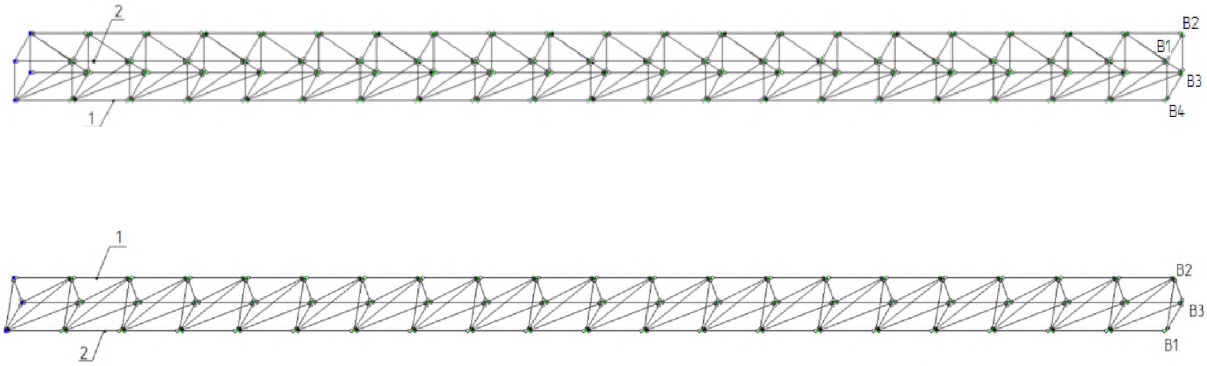

Fig. 8. Design schemes of two types of rods

At a given temperature change $\Delta T = 180$ K maximal permissible rod length

$$l = \frac{10 \cdot 10^{-3}}{180 \cdot 2 \cdot 10^{-6}} = 27.77 \text{ m.}$$

Thus. only the 20 *m* long rod. with both triangular and square cross-section. complies with the specified maximal permissible longitudinal displacement.

Calculations show that displacements perpendicular to the longitudinal axis depend *only* on the dimensions of the cross-section of the rod. and that there is an accumulation of negligible tangential displacements along the cross-section of the rod. especially in places that are not braced.

The resulting rotations of the antenna plane that is attached to the rod. due to its uniform temperature deformation

– for square cross-section do not exceed 0.00036°.
– for triangular cross-section do not exceed 0.00018°.

Based on the above calculations. for uniform thermal deformation. the rotation angle of the antenna plane that is attached to the rod is always equal to the rotation of the end section of the last cell of the rod. and does not depend on the rod length.

The main indicator that affects the amount of rotation of the plane is the stiffness of an individual rod cell. The stiffness of a triangular cell is obviously higher than stiffness of a square cell. as shown by calculations.

Analysis of the influence on geometric reliability of the initial imperfection of rod struts

Consider the influence of the initial imperfection in the length of one rod strut on the position of the attachment points of the antenna to the rod.

Assume for example. the initial imperfection of the belt strut of the second from the attachment point rod cell. There are two types of struts in this cell - incoming and not arriving at the brace attachment point. It is expected that the influence of these two types of struts on the shape of the structure will be different; hence. we consider both cases (Fig. 8).

Define the initial change in rod length as a change in the temperature of a particular strut.

Tables 2 and 3 show the results of calculations of the influence of the initial imperfection of the rod struts on the geometry of the entire spacecraft rod.

Results presented in Tables 2 and 3 shows that displacements of size 1-2 *mm* due to the imperfection of a single strut lead to the same order of displacements as the maximum temperature displacements of the entire structure. Hence. the accuracy of manufacturing individual struts and assembly of nodes is extremely important. The manufacturing culture of telecommunication sputniks has to be in strict accordance with the required accuracy of their initial shape.

Table 2

Calculation results for rod elongation

Rod type	Strut type	Strut length deviation, *mm*	Points	Point displacement. *mm*			Rotation around X-axis, 10^{-4} *radian*
				X-axis	Y-axis	Z-axis	
Square cross-section. length 20 m	1	+1	B1	0	0	26.8657	0.04
			B2	0	0	0	
			B3	0	26.8657	0	
			B4	1	26.8657	26.8657	
		+2	B1	0	0	53.7313	0.08
			B2	0	0	0	
			B3	0	53.7313	0	
			B4	2	53.7313	53.7313	
		+5	B1	0	0	134.328	0.2
			B2	0	0	0	
			B3	0	134.328	0	
			B4	5	134.328	134.328	
	2	+1	B1	1	28.3582	-28.3582	0.042
			B2	0	28.3582	0	
			B3	0	0	0	
			B4	0	0	-28.3582	
		+2	B1	2	56.7164	-56.7164	0.085
			B2	0	56.7164	0	
			B3	0	0	0	
			B4	0	0	-56.7164	
		+5	B1	5	141.791	-141.791	0.211
			B2	0	141.791	0	
			B3	0	0	0	
			B4	0	0	-141.791	
Triangular cross-section. length 20 *m*	1	+1	B1	0	0	-28.3582	0.042
			B2	1	0	-28.3582	
			B3	0	0	-28.3582	
		+2	B1	0	0	-56.7164	0.085
			B2	2	0	-56.7164	
			B3	0	0	-56.7164	
		+5	B1	0	0	-141.791	0.212
			B2	5	0	-141.791	
			B3	0	0	-141.791	
	2	+1	B1	1	26.8657	13.4328	0.02
			B2	0	26.8657	13.4328	
			B3	0	26.8657	13.4328	
		+2	B1	2	53.7313	26.8657	0.04
			B2	0	53.7313	26.8657	
			B3	0	53.7313	26.8657	

Rod type	**Strut type**	**Strut length deviation,** ***mm***	**Points**	**Point displacement.** ***mm***			**Rotation around X-axis,** 10^{-4} ***radian***
				X-axis	**Y-axis**	**Z-axis**	
		+5	B1	5	134.328	67.1642	0.1
			B2	0	134.328	67.1642	
			B3	0	134.328	67.1642	

Table 3

Calculation results for rod shortening

Rod type	**Strut type**	**Strut length deviation,** *mm*	**Points**	**Point displacement. mm**			**Turn around X-axis,** 10^{-4}***radian***
				X-axis	**Y-axis**	**Z-axis**	
Square cross-section. length 20 *m*	1	-1	B1	0	0	-26.8657	0.04
			B2	0	0	0	
			B3	0	-26.8657	0	
			B4	-1	-26.8657	-26.8657	
		-2	B1	0	0	-53.7313	0.08
			B2	0	0	0	
			B3	0	-53.7313	0	
			B4	-2	-53.7313	-53.7313	
		-5	B1	0	0	-134.328	0.2
			B2	0	0	0	
			B3	0	-134.328	0	
			B4	-5	-134.328	-134.328	
	2	-1	B1	-1	-28.3582	28.3582	0.042
			B2	0	-28.3582	0	
			B3	0	0	0	
			B4	0	0	28.3582	
		-2	B1	-2	-56.7164	56.7164	0.085
			B2	0	-56.7164	0	
			B3	0	0	0	
			B4	0	0	56.7164	
		-5	B1	-5	-141.791	141.791	0.211
			B2	0	-141.791	0	
			B3	0	0	0	
			B4	0	0	141.791	
Triangular cross-section. length 20 *m*	1	-1	B1	0	0	28.3582	0.042
			B2	-1	0	28.3582	
			B3	0	0	28.3582	
		-2	B1	0	0	56.7164	0.085
			B2	-2	0	56.7164	

Rod type	Strut type	Strut length deviation, *mm*	Points	Point displacement. mm			Turn around X-axis, 10^{-4}*radian*
				X-axis	Y-axis	Z-axis	
			B3	0	0	56.7164	
		-5	B1	0	0	141.791	0.211
			B2	-5	0	141.791	
			B3	0	0	141.791	
	2	-1	B1	-1	-26.8657	-13.4328	0.02
			B2	0	-26.8657	-13.4328	
			B3	0	-26.8657	-13.4328	
		-2	B1	-2	-53.7313	-26.8657	0.04
			B2	0	-53.7313	-26.8657	
			B3	0	-53.7313	-26.8657	
		-5	B1	-5	-134.328	-67.1642	0.1
			B2	0	-134.328	-67.1642	
			B3	0	-134.328	-67.1642	

Analysis of rod reliability

Determine the reliability of manufacturing a 27-meter-long rod (taken to even count the number of cells of 1 *m*). assuming that the geometrical error during the manufacture of individual sections is determined by the normal distribution function with a given standard deviation (SD).

The geometric limitation of the rod length as stated above is ± 10.0 mm. Exceeding this two-side limit amounts to rod failure as related to antenna performance.

The initial distortion/deformation of the rod cells is considered to be independent from each other; hence. the covariance of the values of the deformation of the rod cells is equal to zero. If the SD of the geometrical error along the X-axis of an individual rod cell is 1 *mm* or 2 *mm*. then the standard deviation of the entire rod length is the sum of the variances of 27 equally distributed random variables RVs

$$\sigma_1 = \sqrt{D[X]} = \sqrt{\sum_{1}^{27} D[X_n]} =$$

$$= \sqrt{27 \cdot 1^2} = 5.196 \text{ mm};$$

$$\sigma_2 = \sqrt{27 \cdot 2^2} = 10.39 \text{ mm}.$$

Reliability. in this case. is the probability that the normally distributed RV of the rod length. depending on the deviation of the cell size. will take values in the interval that satisfies the design limitation on the rod length.

The probabilities for the rod deviation SD equal to 5.196 and 10.39 mm. are. respectively:

$$P(26.99 \le x < 27.01) = F_o\left(\frac{27.01-27}{0.005196}\right) -$$

$$-F_o\left(\frac{26.99-27}{0.005196}\right) = 0.9457;$$

$$P(26.99 \le x < 27.01) = F_o\left(\frac{27.01-27}{0.01039}\right) -$$

$$-F_o\left(\frac{26.99-27}{0.01039}\right) = 0.664.$$

Determine the reliability of the rod for smaller SDs and build a graph of the dependence of rod reliability on the SD of an individual cell length.

Table 4 shows the dependence of the reliability of the rod on the SD of an individual cell and the CD of the entire rod. The graph in Fig. 9 visualizes the resulting dependence.

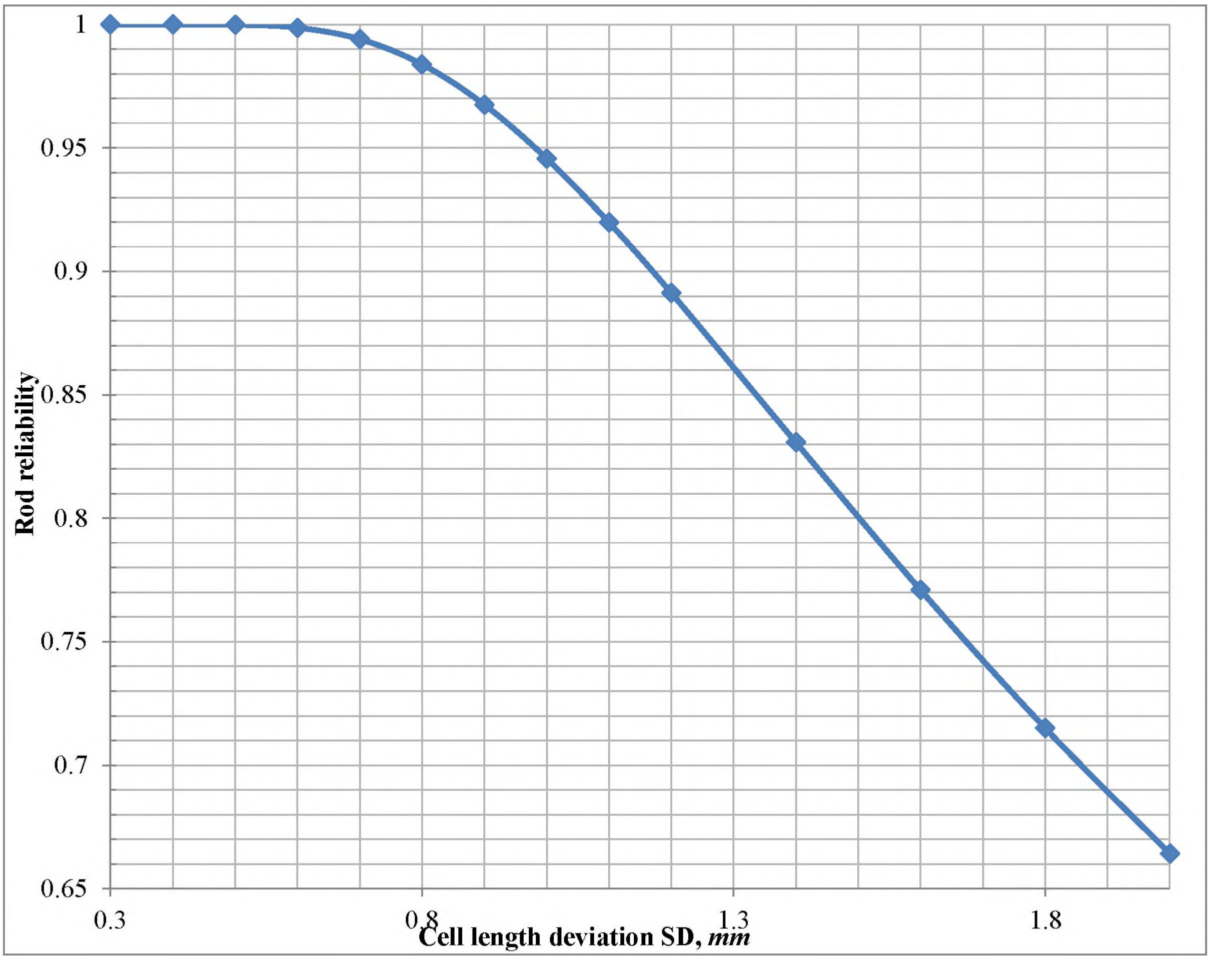

Fig. 9. Dependence of rod reliability on the SD of an individual cell length error

Table 4

Dependence of the rod reliability on the SD

Cell SD, *mm*	**Rod SD, *mm***	**Rod reliability**
2	10.392	0.664090362
1.8	9.353	0.715009478
1.6	8.314	0.770942588
1.4	7.275	0.830735344
1.2	6.235	0.891252712
1.1	5.716	0.919791081
1	5.196	0.945715241
0.9	4.677	0.967493216
0.8	4.157	0.983853226
0.7	3.637	0.994031717
0.6	3.118	0.998659588
0.5	2.598	0.999881455
0.4	2.078	0.999998508
0.3	1.559	1

According to Table 4, reliability calculations outside the SD interval of an individual cell from 0.3 *mm* to 2.0 *mm* are meaningless. since at values of about 0.3 *mm*. the reliability is practically equal to unity. and beyond 2 *mm* it becomes too low for practical use.

It can also be seen from Table 4 and Fig. 9. that the required probability of no-failure operation. equal to 0.999. for a 27 *m* long rod is achieved with a SD deviation of an individual cell length equals 0.5 *mm*.

Approximation the obtained numerical dependence of the reliability on the SD of the cell length by a quadratic function takes the form:

$$R(\sigma) = -0.195\sigma^2 + 0.182\sigma + 0.96. \qquad (*)$$

This function is applicable only in the interval (0.47 ... 1.6) *mm*. Based on the obtained dependence (*). the necessary probability of no-failure operation. equal to 0.999. for a 27*m* long rod is achieved with the SD of an individual cell length equal to 0.6 *mm*.

Conclusion

The paper. to authors' knowledge. is the first attempt to formulate an approach to assessing the geometry-related reliability of a spacecraft structure subjected to temperature cycles loads specific to the stationary orbit of a telecommunication sputnik.

Calculations were performed of the linear displacements of the sputnik antenna-refractor attachment points for two types of rods due to cyclic change in the near-cosmos ambient temperature regime.

The displacements during loading along the Y and Z axes of some points of the antenna attachment plane differ. which indicates a rotation of the attachment plane. This rotation strongly depends on the arrangement of the braces and on the changes of the antenna design as related to the rod proper or its end cell that accommodates the reflector. and these changes could be significant.

The influence of imperfection of an individual structural element on the antenna initial geometry evolution was studied. and an analysis of the geometry-related reliability of the antenna was carried out as a function of the SD of manufacturing geometrical imperfection of an individual rod cell.

The conducted study shows that it is necessary to (1) correctly describe the manufacturing and assembly imperfections of the unique cantilever structure [11] and (2) perform a set of finite element based calculations that would consistently describe the evolution of the initial geometry of the antenna as it is exposed to a sequence of multiple temperature cycles (around 5500) during its operation (12-15 years);

At the same time, it is necessary to take into account all the significant properties of the antenna carbon composite material. such as low cycle fatigue. relaxation. aging. the influence of the environment. etc.

This data will permit assessing the partial geometry-related reliabilities of antenna structure operation. as well as the full reliability of the antenna according to the design limits of antenna geometry distortions.

References

1. Jin. Y. B.-S. Jang Probabilistic fire risk analysis and structural safety assessment of FPSO topside module Ocean Engineering 104 (2015) 725–737.

2. Tsai. S-F. et al. Integrated self-assessment module for fire rescue safety in a chemical plant –A case study.Journal of Loss Prevention in the Process Industries 51 (2018) 137–149.

3. Orozco. J.L et al. Assessment of an ammonia incident in the industrial area of Matanzas. Journal of Cleaner Production 222 (2019) 934-941.

4. SHAO Hui and DUAN Guoning 2012 International Symposium on Safety Science and Technology Risk quantitative calculation and ALOHA simulation on the leakage accident of natural gas power plant .Procedia Engineering 45 (2012) 352 – 359.

5. Ghana gas explosion 'kills five' in Accra: https://www.bbc.com/news/world-africa-38416186 Accessed 21 September. 2019.

6. Khan. F. I.; Amyotte. P. R. Modeling of BP Texas City refinery incident. J. Loss. Prev. Process Ind. 2007. 20. 387−395.

7. Rothermel. R.C.. 1991. Predicting Behavior and Size of crown Fires in the Northern Rocky Mountains. Res. Pap. INT-438. U.S. Department of Agriculture. Forest Service. Intermountain Forest and Range Experiment Station. Ogden. UT. pp. 46.

8. Rothermel. R.C.. 1972. A Mathematical Model for Predicting Fire Spread in Wildland Fuels. Res. Pap. INT- 115. U.S. Department of Agriculture. Forest Service. Intermountain Forest and Range Experiment Station. Ogden. UT. pp. 40.

9. van Wagner. C.E.. 1977. Conditions for the start and spread of crown fire. Can. J. For. Res. 7 (1). 23–34.

10. N. Khakzad et al. Quantitative assessment of wildfire risk in oil facilities. Journal of Environmental Management 223 (2018) 433–443.

11. Khakzad. N.. Khan. F.. Amyotte. P.. Cozzani. V.. 2013. Domino effect analysis using bayesian networks. Risk Anal. 33 (2). 292–306. http://dx.doi.org/10.1111/j. 1539-6924.2012.01854.x.

12. Reniers. G.. 2010. An external domino effects investment approach to improving cross-plant safety within. chemical clusters. J. Hazard. Mater. 177 (1–3). 167–174. http://dx.doi.org/10.1016/j.jhazmat.2009.12.013.

13. Abdolhamidzadeh. B.. Abbasi. T.. Rashtchian. D.. Abbasi. S.A.. 2011. Domino effect in process-industry accidents - an inventory of past events and the identification of some patterns. J. Loss Prev. Process Ind.. http://dx.doi.org/10.1016/j.jlp.2010. 06.013.

14. M.Z. Kamil et al. Dynamic domino effect risk assessment using Petri-nets. Process Safety and

Environmental Protection 124 (2019) 308–316 https://doi.org/10.1016/j.psep.2019.02.019.

15. Bahareh. I.. Berrin. T.. 2015. Explosion impacts during transport of hazardous cargo: GIS-based characterization of overpressure impacts and delineation of flammable zones for ammonia. J. Environ. Manag. 156. 1-9.

16. Shah. T.R.. Tausif. S.. Sultana. R.S.. 2014. Facility layout optimization of on ammonia plant based on risk and economic analysis. In: 10th International Conference on Mechanical Engineering. ICME 2013. Proceedia Engineering. pp. 760–765.

17. VR R. Madhu G. Individual and societal risk analysis and mapping of human vulnerability to chemical accidents in the vicinity of an industrial area.

18. ENERGY COMMISSION ACT. 1997 http://www.energycom.gov.gh/files/ACT.pdf 15 June. 2019

19. Ding L. Khan F. Abbassi R. Ji J. FSEM: an approach to model contribution of synergistic effect of fires for domino effects. Reliability Engineering and System Safety. 2019 Sep;189:271-8.

20. Khakzad N. Khan F. Amyotte P. Cozzani V. Domino effect analysis using Bayesian networks. Risk Analysis: An International Journal. 2013 Feb;33(2):292-306.

21. Alileche N. Olivier D. Estel L. Cozzani V. Analysis of domino effect in the process industry using the event tree method. Safety science. 2017 Aug 1;97:10-9.

22. Cozzani V. Tugnoli A. Salzano E. Prevention of domino effect: From active and passive strategies to inherently safer design. Journal of hazardous materials. 2007 Jan 10;139(2):209-19.

23. Khan FI. Abbasi SA. Major accidents in process industries and an analysis of causes and consequences. Journal of Loss Prevention in the process Industries. 1999 Sep 1;12(5):361-78.

24. Khan FI. Abbasi SA. An assessment of the likelihood of occurrence. and the damage potential of domino effect (chain of accidents) in a typical cluster of industries. Journal of Loss Prevention in the Process Industries. 2001 Jul 1;14(4):283-306.

25. ALOHA software program (https://www.epa.gov/cameo/aloha-software) date accessed 15 June. 2019

26. Tsai SF. Huang AC. Shu CM. Integrated self-assessment module for fire rescue safety in a chemical plant–A case study. Journal of Loss Prevention in the Process Industries. 2018 Jan 1;51:137-49.

27. Chevron Management Failures Led to Massive August 2012 Explosion in Richmond (https://www.eastbayexpress.com/SevenDays/archives/2015/01/29/chevron-management-failures-led-to-massive-august-2012-explosion-in-richmond) date accessed 17-06-2019

28. Deadly Kiev fuel blasts set off blaze near military unit (https://www.yahoo.com/news/gigantic-fire-erupts-fuel-depot-near-kiev-several-073358348.html) date accessed 17-06-2019

29. One injured as massive Kemaman refinery blaze continues to rage [NSTTV] (https://www.nst.com.my/news/nation/2018/07/387904/one-injured-massive-kemaman-refinery-blaze-continues-rage-nsttv) date accessed 18-06-2019.

30. Texas petrochemical fire spreads to more storage tanks after firefighting snag (https://www.cnbc.com/2019/03/19/houston-area-chemical-fire-expected-to-burn-for-days.html) date accessed 20-06-2019.

31. Philadelphia Oil Refinery Explosion Shakes City With Huge Fireball (https://www.nytimes.com/2019/06/21/us/philadelphia-oil-refinery-fire.html) date accessed 23-06-2019.

32. Xu C. Tarko AP. Wang W. Liu P. Predicting crash likelihood and severity on freeways with real-time loop detector data. Accident Analysis & Prevention. 2013 Aug 1;57:30-9.

33. Mohsin M. Zhou P. Iqbal N. Shah SA. Assessing oil supply security of South Asia. Energy. 2018 Jul 15;155:438-47.

34. Bahr NJ. System safety engineering and risk assessment: a practical approach. CRC press; 2018 Oct 8.

35. Wind rose Tema.Greater Accra Region. Ghana. 5.670° N 0.017° W. 27 m asl (https://www.meteoblue.com/en/products/historyplus/windrose/tema_ghana_2294700) date accessed 02-07-2019

36. CPR 18E. 1999. Commission for Prevention of Disasters. Guidelines for Quantitative Risk Assessment. Purple Book. National Institute of Public Health and the Environment (RIVM). Ministry of Transport. Public Works and Water Management. Ministry of Housing. Spatial Planning and the Environment. The Hague. The Netherlands.

37. Antonioni G. Spadoni G. Cozzani V. Application of domino effect quantitative risk assessment to an extended industrial area. Journal of Loss Prevention in the Process Industries. 2009 Sep 1;22(5):614-24.

38. Yaofang F. Shuzhe C. Jing C. Research on virtual reality simulation system of safe navigation environment in Three Gorges Reservoir Area. Procedia Environmental Sciences. 2011 Jan 1;10:331-6.

39. Taghehbaf. M. A.. Givehchi. S.. Ardestani. M.. & Baghvand. A. (2014). Modeling the Consequences of Potential Accidents in One of the Gasoline Storage Tanks at Oil Storage of Yazd. in Terms of Explosion. 557-559.

40. Kardell L. Lööf M. QRA with respect to domino effects and property damage. Gas. 2014;50(300):1000.

41. Reniers GL. Dullaert W. DomPrevPlanning©: User-friendly software for planning domino effects prevention. Safety Science. 2007 Dec 1;45(10):1060-81.

42. Cozzani V. Antonioni G. Landucci G. Tugnoli A. Bonvicini S. Spadoni G. Quantitative assessment of domino and NaTech scenarios in complex industrial areas. Journal of Loss Prevention in the Process Industries. 2014 Apr 11;28:10-22.

43. FLACS Software (http://www.gexcon.com/products-services/FLACS-Software/22/en) date accessed 15-10-2019.

44. PHAST and SAFETI - DNV GL Software program (https://www.dnvgl.com/services/quantitative-risk-analysis-software-safeti-1715) date accessed 15-10-2019.

45. TOXI+Risk Software program (https://toxi.ru/produkty/programmnyi-kompleks-toxirisk-5) date accessed 15-10-2019.

30. Yasvin V.A. Obrazovatel'naya sreda: ot modelirovaniya k proektirovaniyu [Educational environment: from modeling to design]. Moscow, Smysl, 2001, 365 p. (In Russ.).

31. Gerchenfeld N. et al. The Internet of things. Scientific American, 2004, no. 291, pp. 76-81.